Eur. Phys. J. C 7, 225–232 (1999)
DOI 10.1007/s100529801006

THE EUROPEAN PHYSICAL JOURNAL C


# Three jet cross sections in photoproduction at HERA

M. Klasen

High Energy Physics Division, Argonne National Laboratory, Argonne, Illinois 60439, USA (e-mail: klasen@hep.anl.gov)

Received: 5 August 1998 / Published online: 19 October 1998

**Abstract.** We calculate three jet cross sections in photoproduction using exact matrix elements for the direct and resolved contributions. Numerical distributions are presented in a generic, irreducible set of variables that allows to disentangle the dynamics of partonic QCD subprocesses from each other and from pure phase space distributions. The results are compared to preliminary data from the ZEUS collaboration at HERA. It is found that the largest contribution comes from photon-gluon fusion in the mass range 36 GeV $< M_{3-\mathrm{jet}} <$ 80 GeV. The measured leading jet scattering angle distribution is consistent with the $t$-channel exchange of a massless fermion in $2 \to 2$ scattering, where the third parton is assumed to arise from soft bremsstrahlung. The data are inconsistent with pure phase space and Rutherford scattering distributions.

## 1 Introduction

Photoproduction of jets has been studied to a great extent at HERA since the DESY electron-proton collider turned on in 1992 by the H1 [1] and ZEUS [2] collaborations. Until recently, however, the limited luminosity only allowed for measuring inclusive single jet and dijet cross sections. In general, the data have shown good agreement with QCD predictions accurate to next-to-leading order in perturbation theory [3]. They have confirmed the existence of direct and resolved partonic contributions for real and slightly off-shell photons and begin to show sensitivity to different parametrizations of the parton densities in the photon provided that uncertainties from the underlying hadronic event and the jet definition are under control [4,5].

On the other hand, multijet production has been measured some time ago in purely hadronic collisions at the CERN SPS collider by the UA1 collaboration [6] and at the Fermilab Tevatron collider by the CDF [7] and D0 [8] collaborations. Its importance lies not only in testing perturbative QCD to higher orders, but also in the search for new phenomena. Many analyses for the production of Standard Model and new particles, e.g. the top quark, the Higgs boson, or supersymmetric particles, rely on many hard jets in the final state. QCD multijet production then is a significant background for these searches and has to be well understood.

At HERA the single jet transverse energy and dijet mass distributions in photoproduction have shown no deviations from the next-to-leading order QCD predictions so far. However, higher integrated luminosity has now permitted ZEUS to produce the first three jet analysis [9]. Even a limited number of four jet events has been observed. It is therefore interesting to compare these new data with QCD predictions and look for deviations as signals of new physics. Since next-to-leading order cross sections for the photoproduction of three jets are not available, such an analysis is still restricted to leading order in perturbation theory and will therefore be subject to large renormalization and factorization scale uncertainties. As a possible way out, we will concentrate in this paper on normalized distributions that are largely independent of both higher order corrections and scale choices as are the shapes of the distributions. We briefly review the leading order cross section formalism and the relevant kinematic variables before we present numerical results for both dynamic QCD and pure kinematic phase space distributions. We disentangle the different partonic subprocesses that contribute to photoproduction of three jets and show that the leading jet scattering angle distribution in three jet production is closely related to two jet production.

The paper is organized as follows: In Sect. 2, we briefly review the leading order $2 \to 3$ parton scattering processes. In Sect. 3 we define the relevant phase space variables and the hadronic three jet cross sections. Our numerical results are presented in Sect. 4, and we summarize our analysis in Sect. 5.

## 2 Leading order $2 \to 3$ parton scattering

Our predictions for three jet cross sections in photoproduction are based on the leading order $2 \to 3$ matrix elements $\overline{|\mathcal{M}|^2}$ averaged over initial and summed over final spin and color states. The partonic cross section can then be calculated through

$$\sigma_{12}^{345} = \frac{1}{2s}\overline{|\mathcal{M}|^2}(2\pi)^4\delta(p_1+p_2-p_3-p_4-p_5) \times \prod_{i=3}^{5}\frac{\mathrm{d}^4p_i}{(2\pi)^3}\delta(p_i^2)\ . \quad (1)$$

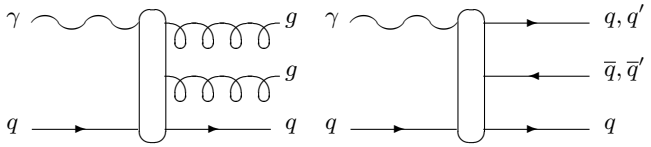


**Fig. 1.** Leading order $2 \to 3$ Feynman diagrams for direct photoproduction

We denote the four-momenta of the incoming and outgoing partons by $p_{1,2}$ and $p_{3,4,5}$ and the partonic center-of-mass energy squared by $s = (p_1 + p_2)^2$.

Both direct and resolved processes have to be taken into account. The generic diagrams for direct $2 \to 3$ scattering, where the photon interacts directly with a parton in the proton, are displayed in Fig. 1. These diagrams arise from the leading order $2 \to 2$ QCD Compton scattering process

$$\overline{|\mathcal{M}|^2}_{\gamma q \to qg} = 16\pi^2 \alpha \alpha_s 2 C_F \left( -\frac{s}{t} - \frac{t}{s} \right) \tag{2}$$

through the emission of an additional gluon (left diagram in Fig. 1) or the splitting of the final state gluon into a quark-antiquark pair (right diagram in Fig. 1). $\alpha$ and $\alpha_s$ denote the electromagnetic and strong coupling constants, $s$, $t$, and $u$ are the usual Mandelstam variables for $2 \to 2$ scattering, and $C_F = (N_C^2 - 1)/(2N_C)$ with $N_C = 3$ is the SU(3) color factor. It is worth noting that both the QCD Compton and the crossed photon-gluon fusion processes proceed through a massless fermion exchange in the $t$-channel, which leads to a single $1/t$ pole in the matrix element. Both diagrams in Fig. 1 lead to an extra factor of $\alpha_s$, when the matrix elements are squared, so that the direct $2 \to 3$ cross sections are of $\mathcal{O}(\alpha \alpha_s^2)$. The outgoing quark-antiquark pair can be of the same or different flavor than the incoming quark. The diagrams for incoming antiquarks or gluons can be obtained from Fig. 1 by crossing a final quark or gluon line with the incoming quark line. All possible topologies and orders of outgoing particles have to be considered for the full matrix elements of the processes, although they are not shown here explicitly. The complete result in $d$ dimensions can be found in [10] in a very compact notation. Since there are no singularities present in three jet production, we can simply set $d = 4$.

If the photon resolves into its partonic content before the hard scattering takes place, the effective hard scattering is of purely partonic nature. The relevant generic diagrams are displayed in Fig. 2. They are of $\mathcal{O}(\alpha_s^3)$ and arise from the underlying $2 \to 2$ parton-parton scattering processes through radiation of an additional gluon in the final state. Most of the $2 \to 2$ parton-parton processes proceed through the exchange of a massless vector boson in the $t$-channel leading to a double pole $1/t^2$ in the matrix elements. For example, the matrix element for the process $qq' \to qq'$ is given by

$$\overline{|\mathcal{M}|^2}_{qq' \to qq'} = 16\pi^2 \alpha_s^2 \frac{C_F}{N_C} \frac{s^2 + u^2}{t^2}. \tag{3}$$

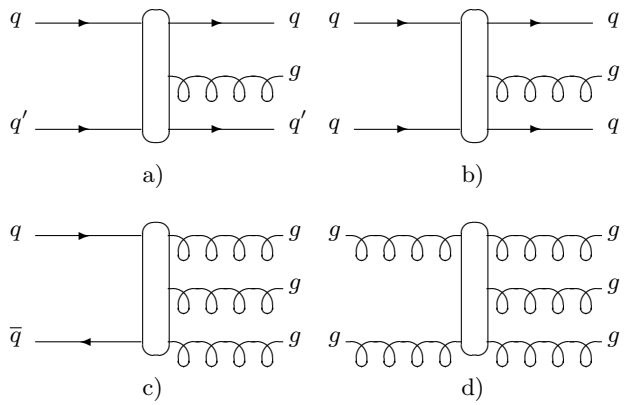


**Fig. 2.** Leading order $2 \to 3$ Feynman diagrams for resolved photoproduction

Crossing one or two outgoing gluon lines into the initial state in Fig. 2 leads to the gluon initiated processes with quarks in the final state, and crossing an incoming and outgoing quark line leads to the processes with incoming anti-quarks. Process c) is symmetric under the interchange of the three gluons and under the interchange of the quark and anti-quark. Process d) is completely symmetric under the interchange of any of the five gluons. The complete result for the $2 \to 3$ parton scattering matrix elements in $d$ dimensions can be found in [11], where we can set $d = 4$ again.

## 3 Hadronic three jet cross sections

At HERA, positrons and protons are currently collided with energies of $E_e = 27.5$ GeV and $E_p = 820$ GeV. The hadronic three jet cross section can be calculated from the partonic cross section $\sigma_{12}^{345}$ with the help of the factorization theorem,

$$\sigma_{ep}^{3-\text{jet}}(s_H) = \int \mathrm{d}x_e f_e(x_e, M^2) \mathrm{d}x_p f_p(x_p, M^2) \times \sigma_{12}^{345}(x_e x_p s_H, M^2). \tag{4}$$

$M$ is the factorization scale and $\sqrt{s_H} = \sqrt{(p_e + p_p)^2} = 300$ GeV is the hadronic center-of-mass energy. $f_e$ denotes the parton density in the positron and is given by a convolution of the density of photons in the positron with the density of partons in the photon,

$$f_e(x_e, M^2) = \int \frac{\mathrm{d}y}{y} f_e^\gamma(y) f_\gamma^{\gamma,q,g}(x_e/y, M^2). \tag{5}$$

$f_e^\gamma(y)$ is given by the Weizsäcker-Williams-Approximation [12], and we include the subleading terms calculated in [13]. Experimentally the photon has a virtuality of $Q < 1$ GeV and carries a fraction $0.2 < y < 0.8$ of the positron energy. For the parton densities in the photon $f_\gamma^{\gamma,q,g}$ and proton $f_p^{q,g}$, we use the leading order parametrizations by GRV [14] and CTEQ4 [15] except where stated otherwise.

Asymptotically, the parton densities in the photon are of $\mathcal{O}(\alpha/\alpha_s)$, so when they are convoluted with the resolved $2 \to 3$ matrix elements of $\mathcal{O}(\alpha_s^3)$, the hadronic cross section is of the same order as the direct contribution. The strong coupling constant $\alpha_s(\mu)$ is calculated in the one-loop approximation with five flavors and $\Lambda^{(5)} = 181$ MeV as found in the global fit of the parton densities in the proton. The renormalization and factorization scales are set to the maximum transverse jet energy in the event, $\mu = M = \max(E_{T,1}, E_{T,2}, E_{T,3})$.

In the ZEUS three jet analysis, jets are defined by the KTCLUS algorithm in inclusive mode [16]. This definition uses a parameter $R = 1$ and combines two hadronic clusters $i$ and $j$ if

$$d_{ij} = \min\left(E_{T,i}^2, E_{T,j}^2\right)\left[(\eta_i - \eta_j)^2 + (\phi_i - \phi_j)^2\right]/R^2 \quad (6)$$

is smaller than

$$d_i = E_{T,i}^2. \quad (7)$$

The transverse energy $E_T$, pseudorapidity $\eta$, and azimuthal angle $\phi$ of the combined cluster are calculated from the transverse energy weighted sums of the two preclusters,

$$E_T = E_{T,i} + E_{T,j}, \quad (8)$$
$$\eta = [E_{T,i}\eta_i + E_{T,j}\eta_j]/E_T, \quad (9)$$
$$\phi = [E_{T,i}\phi_i + E_{T,j}\phi_j]/E_T. \quad (10)$$

The longitudinal momentum fractions $x_p$ and $x_e$ of a parton in the proton and electron can be determined from the observed three jet final state through four momentum conservation

$$x_{p,e} = \sum_{i=3}^{5} E_{T,i} e^{\pm\eta_i}/\sqrt{s_H}, \quad (11)$$

where the plus sign applies to the proton going into the positive $z$ direction and the jet pseudorapidities $\eta_i$ are defined in the center-of-mass frame. The longitudinal momentum fraction of a parton in the photon is given by $x_\gamma = x_e/y$. The three jets are required to have transverse energies of $E_{T,3}, E_{T,4} > 6$ GeV and $E_{T,5} > 5$ GeV, and their pseudorapidities must lie within $|\eta_{3,4,5}| < 2.4$ in the laboratory frame [9]. The KTCLUS algorithm is favored experimentally and in higher order theoretical predictions since it contains no overlap or double counting ambiguities. Leading order QCD predictions, however, lack the possibility to implement or distinguish a particular jet definition, since each parton is identified with a jet.

For $N$ massless jets, one can choose $3N-4$ parameters that should span the multijet parameter space, facilitate a simple interpretation within QCD, and allow for a comparison of the $N-1$-jet to the $N$-jet cross section. In the case of $N = 3$, the conventional choices are the three jet mass $M_{3-\mathrm{jet}}$, required by ZEUS to be larger than 50 GeV, and four dimensionless parameters. The Dalitz energy fractions

$$x_i = \frac{2E_i}{M_{3-\mathrm{jet}}} \quad (12)$$

specify how the available energy is shared between the three jets. They are ordered such that $x_3 > x_4 > x_5$. Since $x_3 + x_4 + x_5 = 2$, only $x_3$ and $x_4$ are linearly independent. The third and fourth parameters are the cosine of the scattering angle between the leading jet and the average beam direction $\mathbf{p}_{\mathrm{AV}} = \mathbf{p_1} - \mathbf{p_2}$, where the incoming parton 1 is the one with the highest energy in the laboratory frame,

$$\cos\theta_3 = \frac{\mathbf{p}_{\mathrm{AV}}\mathbf{p_3}}{|\mathbf{p}_{\mathrm{AV}}||\mathbf{p_3}|}, \quad (13)$$

and the angle between the three jet plane and the plane containing the leading jet and the beam direction,

$$\cos\psi_3 = \frac{(\mathbf{p_3} \times \mathbf{p}_{\mathrm{AV}})(\mathbf{p_4} \times \mathbf{p_5})}{|\mathbf{p_3} \times \mathbf{p}_{\mathrm{AV}}||\mathbf{p_4} \times \mathbf{p_5}|}. \quad (14)$$

Instead of $\cos\psi_3$ we will investigate distributions in $\psi_3$ itself. In the soft limit, where $E_5 \to 0$ and $x_{3,4} \to 1$, $\cos\theta_3$ approaches the $2 \to 2$ center-of-mass scattering angle $\cos\theta^*$ thus relating three jet to two jet cross sections. $\cos\theta^*$ can be determined from the pseudorapidities of the two jets by

$$\cos\theta^* = \tanh\left(\frac{\eta_3 - \eta_4}{2}\right) \quad (15)$$

and is related to the $2 \to 2$ Mandelstam variables by

$$t = -\frac{1}{2}s(1 - \cos\theta^*) \quad \text{and} \quad u = -\frac{1}{2}s(1 + \cos\theta^*). \quad (16)$$

Of course, the third jet must not be too soft (or the hard jets not too hard) to avoid soft singularities that would have to be absorbed into the next-to-leading order dijet cross section. This is achieved by a cut on $x_3 < 0.95$. However, since the energy of a jet is always larger than its transverse energy, the cut on $E_{T,5} > 5$ GeV already insures the absence of soft singularities. The three jets also have to be well separated in phase space from each other and from the incident beams to avoid initial and final state collinear singularities. This is insured by a cut on $|\cos\theta_3| < 0.8$, by the cuts in the pseudorapidities, and by the isolation cuts in the jet definition.

## 4 Numerical results

Having explained the relevant theoretical details in the last two sections, we can now turn to the presentation of numerical results for the photoproduction of three jets at HERA. We first look for discrepancies between theory and ZEUS data [9] in the three jet mass distribution in Fig. 3. We find that the total theoretical prediction (full curve) describes the data well in shape and normalization. The agreement in normalization is, however, to some degree coincidental since there is still an uncertainty of a factor of two from the variation of the scales $\mu = M \in [0.5; 2.0] \times \max(E_{T,3}, E_{T,4}, E_{T,5})$ (shaded band). This theoretical uncertainty is much bigger than the statistical experimental error of about 5% at small $M_{3-\mathrm{jet}}$ indicating the need to implement next-to-leading order

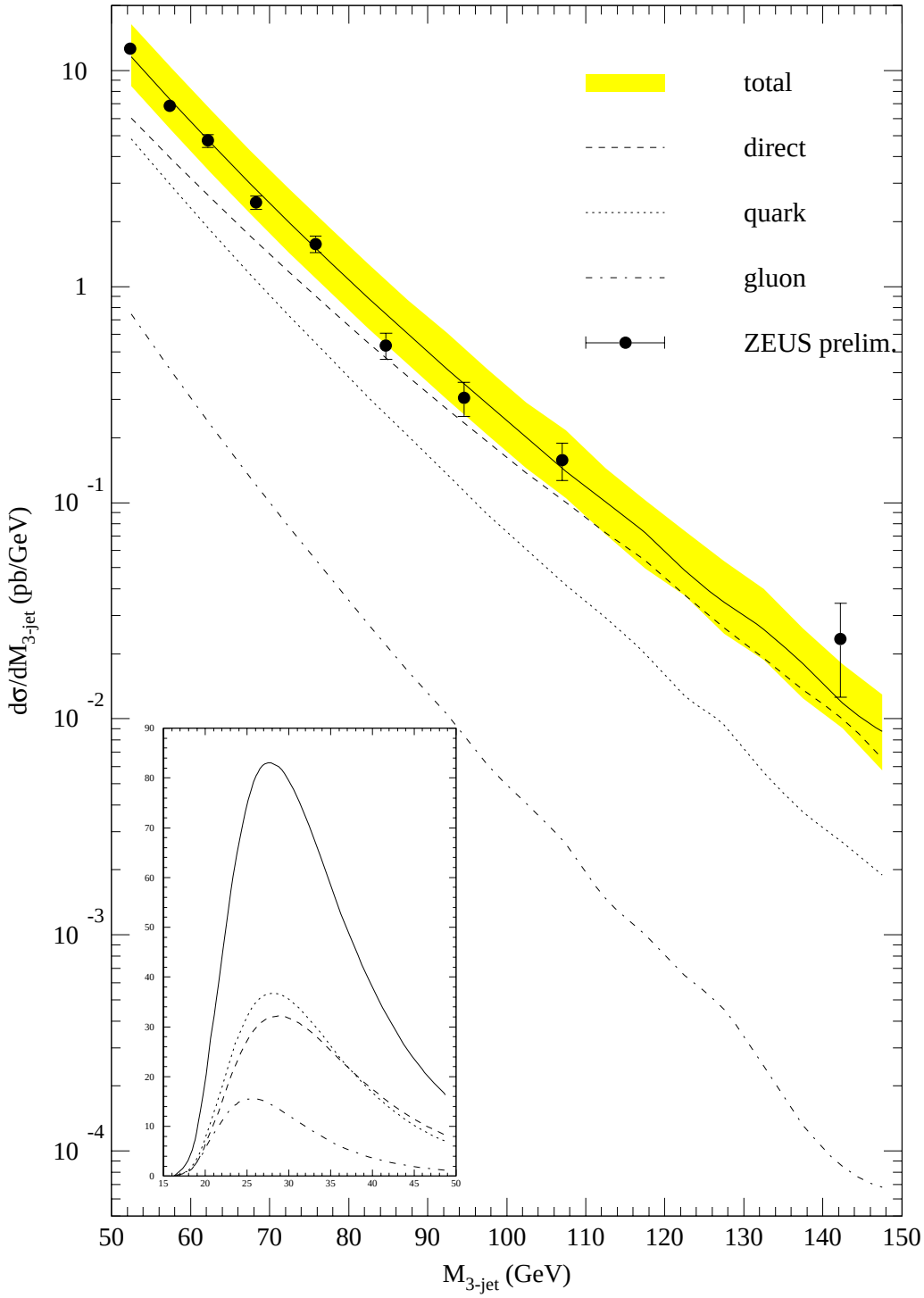


**Fig. 3.** Total cross section (*full curve*) for the photoproduction of three jets as a function of the three jet mass $M_{3-\mathrm{jet}}$. We also show the variation of the absolute normalization due to the uncertainty in the scale choice (*shaded band*) and the contributions from direct photons (*dashed*), quarks (*dotted*), and gluons (*dot-dashed*) in the photon. The ZEUS data [9] agree well with the QCD prediction in shape and normalization within the statistical error

corrections in the three jet cross section. Since these are not available yet, we will subsequently resort to normalized distributions that are largely independent of both higher order corrections and scale choices. In Fig. 3 we also show the individual contributions to the total cross section by direct photons (dashed curve, contributes more than 50%), by quarks (dotted curve, contributes less than 40%), and by gluons (dot-dashed curve, contributes less than 10%) in the photon. From the inset smaller figure it becomes clear that the quark-initiated process gives the largest contribution for $M_{3-\mathrm{jet}} < 36$ GeV. We also computed but do not show here the individual contributions from quarks and gluons in the proton and find the gluon to give the largest contribution for $M_{3-\mathrm{jet}} < 80$ GeV. In

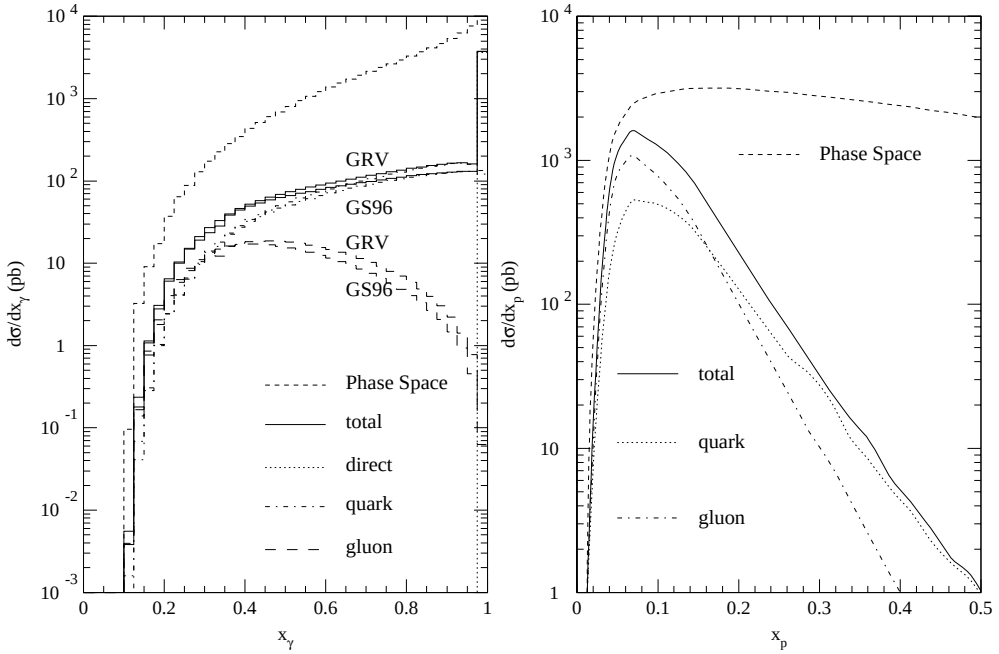


**Fig. 4.** Total three jet cross sections per bin (full curves) as functions of the longitudinal momentum fraction $x_\gamma$ of a direct photon (*dotted*), quark (*dot-dashed*), or gluon (*long-dashed*) in the photon (*left*) and of the longitudinal momentum fraction $x_p$ of a quark (*dotted*) or gluon (*dot-dashed*) in the proton (*right*). Also shown are the pure phase space distributions (*dashed curves*) which differ clearly from the dynamical QCD distributions

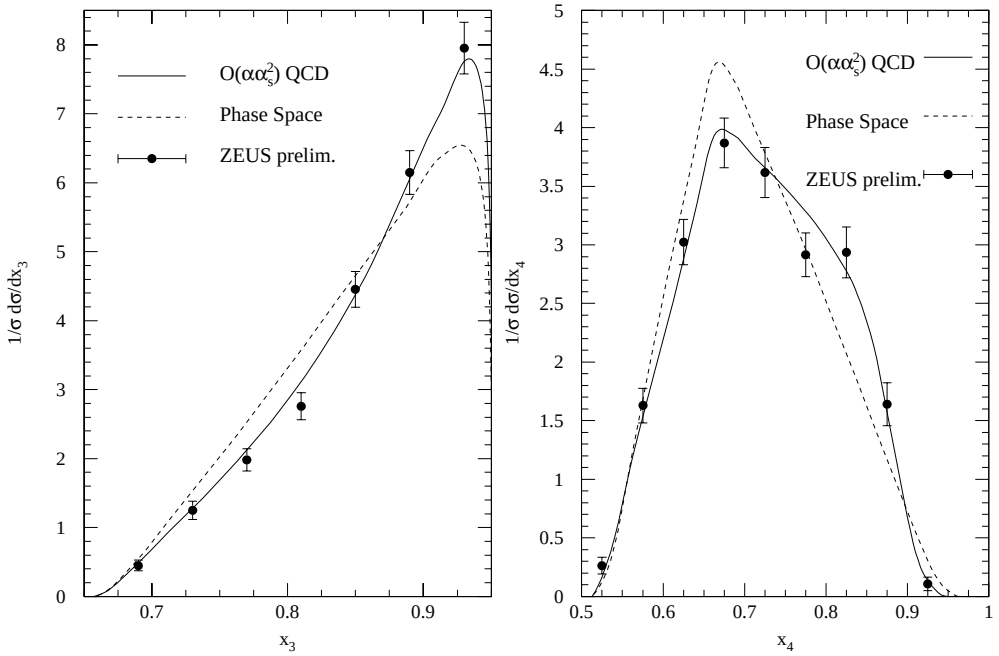


**Fig. 5.** Dependence of the total cross section (*full curves*) and phase space (*dashed curves*) on the energy fractions $x_3$ (*left*) and $x_4$ (*right*) of the leading and next-to-leading jets. The ZEUS data [9] show a slight preference of the full QCD prediction over phase space

the region of 36 GeV $< M_{3-\mathrm{jet}} <$ 80 GeV, the photon-gluon fusion process accounts for one third of the total cross section.

In Fig. 4, we show the total three jet cross section per bin as a function of the longitudinal momentum fractions $x_\gamma$ of the partons in the photon (left) and $x_p$ of the partons in the proton (right). These distributions reflect the situation near the cut at $M_{3-\mathrm{jet}} > 50$ GeV, since the three jet cross section falls off exponentially with the three jet mass. In the left figure, the total cross section (full curve) is presented together with the direct peak at $x_\gamma = 1$ (dotted), which has been divided by the bin width, and the quark (dot-dashed) and gluon (long-dashed) initiated processes. The kinematic cuts restrict the phase space to $x_\gamma > 0.1$ (dashed). The quark initial state is bigger than the gluon above $x_\gamma = 0.3$, and both contributions are larger (smaller) in the GRV parametrization than in GS96 [17] when $x_\gamma > 0.35$ ($x_\gamma < 0.35$). For the longitudinal momentum fraction $x_p$ of the parton in the proton (right side of Fig. 4), the kinematic cuts restrict the phase space to

$x_p > 2.5 \cdot 10^{-2}$ and render contributions above $x_p > 0.5$ insignificant. The gluon (quark) in the proton dominates for $x_p < 0.16$ ($x_p > 0.16$), and at low three jet masses, the gluon contributes about two thirds of the total cross section.

We now turn to normalized distributions in the four dimensionless three jet parameters $x_3, x_4, \cos\theta_3$, and $\psi_3$. Some of the theoretical predictions have already been included in the presentation of the experimental data [9]. Figure 5 shows the three jet cross section as a function of the energy fractions of the leading (left) and next-to-leading (right) jet $x_3$ and $x_4$, normalized to the total cross section. The prediction from the $\mathcal{O}(\alpha\alpha_s^2)$ QCD matrix elements (full curves) are rather similar to the pure phase space distributions (dashed curves), but the data slightly prefer the QCD predictions. The statistical error bars are still too large for a definite conclusion, however. We have also studied the relative contributions from the different partonic sub-channels. They are flat in $x_3$, but photon-quark scattering clearly dominates when $x_4 \simeq x_3 \to 1$.

The distribution in the cosine of the scattering angle of the fastest jet $\cos\theta_3$ is displayed in the lower plot of Fig. 6 together with the distribution in the dijet scattering angle $\cos\theta^*$ (upper plot) measured earlier by ZEUS [5] and compared to theoretical predictions in [3]. They are both of $\mathcal{O}(\alpha\alpha_s^2)$ which is the leading order for the three jet case but next-to-leading order for the dijet case. The wiggles in the latter stem from limited statistics in the Monte Carlo integration. Of course, the cuts in the dijet and three jet cross sections differ slightly, but the most important cuts on the jet mass $M_{2-\mathrm{jet}} > 47$ GeV and the scattering angle $|\cos\theta^*| < 0.8$ are in fact very similar. The differences will also mainly affect the normalization and should be insignificant in distributions normalized at $\cos\theta = 0$ as they are presented here. Let us first concentrate on the dijet case. As expected it is symmetrical in $\cos\theta^*$. The data show good agreement with the QCD prediction (full curve) but clearly disagree with the pure phase space distribution (dashed curve). It might be surprising at first sight that the data also disagree with the Rutherford scattering form at small angle, $(1-|\cos\theta^*|)^{-2}$. On the other hand, the data agree very well with the less singular form $(1-|\cos\theta^*|)^{-1}$. This can be understood if we remind ourselves that Rutherford scattering is characteristic of the exchange of a massless vector boson in the $t$-channel

$$\overline{|\mathcal{M}|^2} \propto t^{-2} = \left[-\frac{1}{2}s(1-\cos\theta^*)\right]^{-2} \qquad (17)$$

as present in most of the resolved (parton-parton) scattering processes whereas both direct processes proceed through a massless *fermion* exchange in the $t$-channel with less singular behavior,

$$\overline{|\mathcal{M}|^2} \propto t^{-1} = \left[-\frac{1}{2}s(1-\cos\theta^*)\right]^{-1}. \qquad (18)$$

In addition, the process $\gamma q \to qg$ has an $s$-channel contribution without any singular behavior. Therefore, the

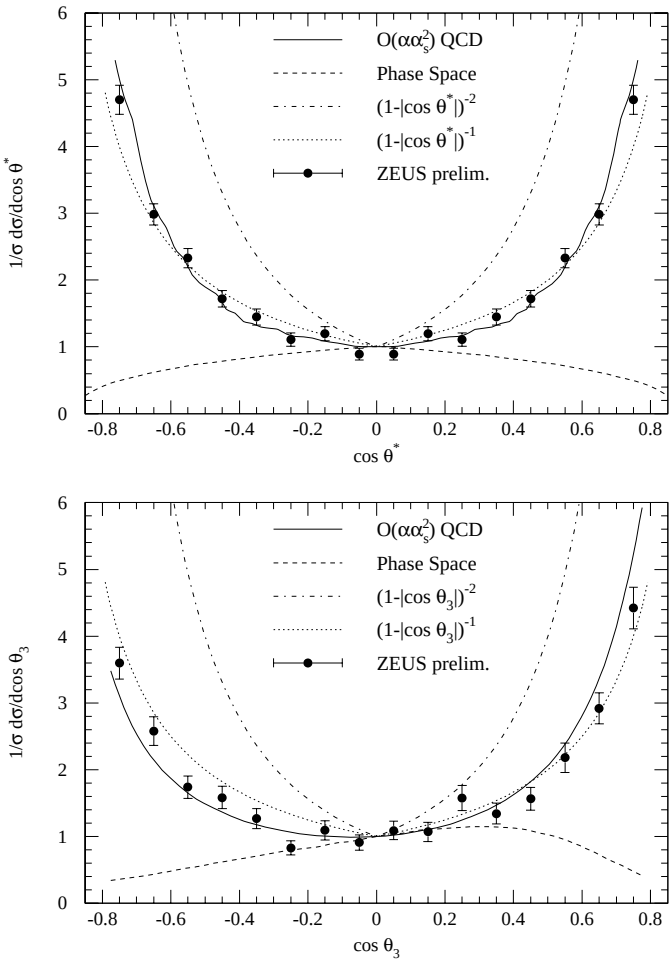


**Fig. 6.** Cross sections for the photoproduction of two (*upper plot*) and three (*lower plot*) jets as functions of the center-of-mass and fastest jet scattering angles normalized at $\cos\theta = 0$. The ZEUS dijet [5] and three jet data [9] are well described by the QCD predictions (*full curves*), but not by the pure phase space distributions (*dashed curves*), and they favor the single $1/t$ pole for massless fermion exchange (*dotted curves*) over the double $1/t^2$ pole for massless boson exchange (*dot-dashed curves*) in the $t$-channel

$\cos\theta^*$ distribution provides evidence that direct processes and photon-gluon fusion in particular are the most important subprocesses in this kinematic region. Turning now to the three jet cross section, we observe that both the $\mathcal{O}(\alpha\alpha_s^2)$ QCD (full curves) and phase space distributions (dashed curves) are asymmetric in $\cos\theta_3$ which motivates why we kept the sign in the abscissa and did not present curves in the absolute value $|\cos\theta|$ as one usually does in the dijet case. Again the data clearly prefer QCD (full) over phase space (dashed) and the single pole in $t$ (dotted) over the double pole (dot-dashed). In fact, the dependence of the three jet cross section on the scattering angle of the fastest jet is strikingly similar to the dijet distribution in the center-of-mass scattering angle. The deviation in the backward region of the three jet case $\cos\theta_3 < 0$, when the pseudorapidity of the fastest jet $\eta_3 < \eta_{4,5}$ is tending towards the direction of the photon beam, can be traced to

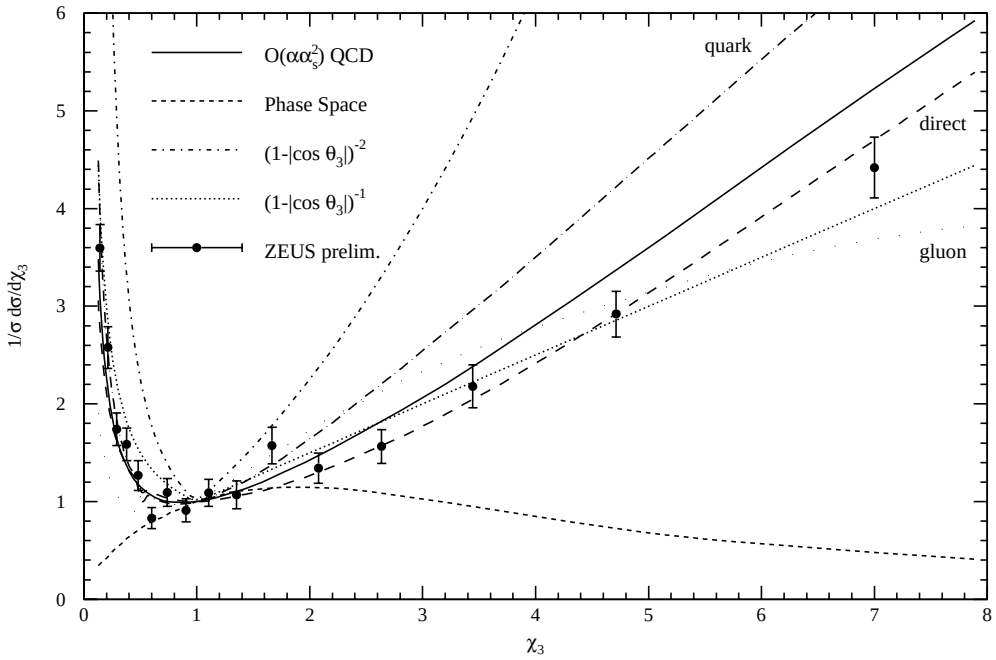


**Fig. 7.** Dependence of the total three jet cross section on the angular variable $\chi_3$. The ZEUS data [9] agree with the QCD prediction (*full curve*), which is dominated by the direct contribution (*long-dashed*), and with the single pole in $t$ (*dotted*). They exclude the pure phase space (*dashed*), quark (*long-dash-dotted*) and gluon (*wide-dotted*) initiated distributions as well as the double pole in $t$ (*dot-dashed*)

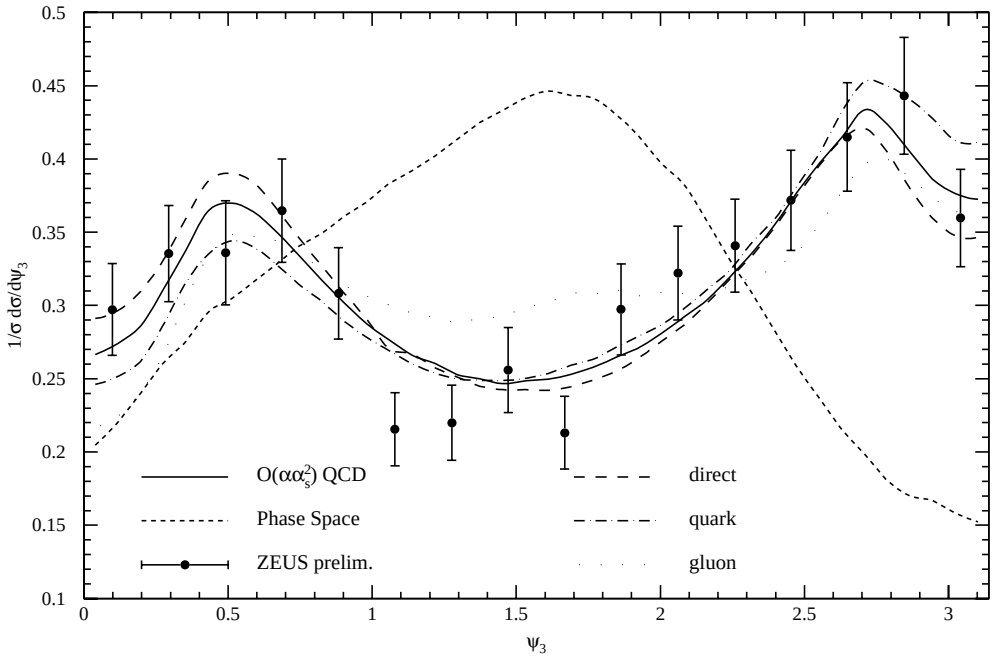


**Fig. 8.** Dependence of the total three jet cross section (*full curve*), the pure phase space (*dashed curve*), and the individual contributions from the partons in the photon (*long-dashed, long-dash-dotted,* and *wide-dotted curves*) on the angle between the three jet plane and the plane containing the leading jet and the average beam direction. The ZEUS data [9] rule out the pure phase space and gluon initiated distributions

a large extent to the asymmetric phase space. Since three jet production proceeds dominantly through single gluon bremsstrahlung, we can relate this result to the underlying $2 \to 2$ process with the interpretation given there. In fact it is interesting to note that the CDF collaboration compared their first three jet data directly to two jet predictions when three jet predictions were still unavailable [18].

To study deviations from the $(1-\cos\theta)^{-2}$ behavior it is convenient to plot the data in terms of the variable [19]

$$\chi = \frac{1+\cos\theta}{1-\cos\theta} \tag{19}$$

which is related to the experimentally measured pseudorapidities by

$$\chi = e^{\eta_1 - \eta_2} \tag{20}$$

and removes the Rutherford singularity such that

$$\frac{\mathrm{d}\sigma}{\mathrm{d}\chi} \sim \text{constant} \tag{21}$$

if one ignores the angular dependence and scaling violation in the coupling constant and the parton densities. In Fig. 7 we present distributions in the angular variable $\chi$ of the fastest of three jets, normalized at $\chi = 1$ (i.e. $\cos\theta = 0$). The data show again a clear distinction from both pure phase space and Rutherford scattering at small angle $(1-|\cos\theta|)^{-2}$ but agree very well with $\mathcal{O}(\alpha\alpha_s^2)$ QCD prediction and also with the form $(1-|\cos\theta|)^{-1}$. The QCD prediction includes, of course, scaling violation both in the strong coupling and in the parton densities. Absence of scaling violations would result in a constant prediction and would clearly disagree with the data. As before, the full QCD prediction is dominated by direct photon scattering. Therefore the long-dashed curve lies close to the full curve, whereas the processes initiated by the quark in the photon (long-dash-dotted curve) give a steeper shape as expected. The gluon initiated processes (wide-dotted curve) have an even different shape. The total resolved contribution (not shown), i.e. the sum of quark and gluon initiated contributions, lies between the quark initiated and total curves and accounts for the remaining difference of the direct initiated and total cross section.

Finally we investigate the dependence of the three jet cross section normalized to the total cross section on the angle between the three jet plane and the plane containing the leading jet and the average beam direction in Fig. 8. The full QCD curve again agrees well with the data as do the contributions from direct photons (long-dashed curve) and quarks in the photon (long-dash-dotted curve), whereas the pure phase space (dashed curve) has a completely different shape. The gluon in the photon (wide-dotted curve) gives a slightly different shape.

## 5 Summary

In this paper we have presented three jet cross sections in photoproduction using exact leading order matrix elements. The normalization and shape of the QCD predictions show good agreement with ZEUS data, although the normalization is subject to rather large scale uncertainties. None of the distributions can be explained by the three jet phase space alone. Of the different direct and resolved contributions, direct and in particular photon-gluon fusion processes are the most important subprocesses. The fastest-jet scattering angle distribution looks very similar to the dijet center-of-mass scattering angle distribution indicating that three jet production proceeds mainly through single bremsstrahlung. The data are not consistent with Rutherford scattering for the exchange of a massless boson but with the less singular form for the exchange of a massless fermion in the $t$-channel.

*Acknowledgements.* Work in the High Energy Physics Division at Argonne National Laboratory is supported by the U.S. Department of Energy, Division of High Energy Physics, Contract W-31-109-ENG-38. The author thanks Laurel Sinclair and Esther Strickland for making the preliminary ZEUS data available to him and Gustav Kramer for useful comments on the manuscript.

## References

1. H1 Collaboration (T. Ahmed et al.), Phys. Lett. B **297**, 205 (1992)
2. ZEUS Collaboration (M. Derrick et al.), Phys. Lett. B **297**, 404 (1992)
3. M. Klasen, T. Kleinwort, G. Kramer, Eur. Phys. J. direct C **1**, 1 (1998) and references therein
4. H1 Collaboration (C. Adloff et al.), Eur. Phys. J. C **1**, 97 (1998)
5. ZEUS Collaboration (M. Derrick et al.), Talk given at the International Conference on High Energy Physics, Jerusalem (1997), N-654
6. UA1 Collaboration (G. Arnison et al.), Phys. Lett. **158B**, 494 (1995)
7. CDF Collaboration (F. Abe et al.), Phys. Rev. D **45**, 1448 (1992); Phys. Rev. Lett. **75**, 608 (1995); Phys. Rev. D **54**, 4221 (1996)
8. D0 Collaboration (S. Abachi et al.), Phys. Rev. D **53**, 6000 (1996); Phys. Lett. B **414**, 419 (1997)
9. L.E. Sinclair for the ZEUS Collaboration, Talks given at the International Conference on High Energy Physics, Vancouver (1998), Abstract 800, and at the 6th International Workshop on Deep Inelastic Scattering and QCD (DIS '98), Brussels, Belgium, April 4-8, 1998, hep-ex/9805010
10. P. Aurenche, R. Baier, A. Douiri, M. Fontannaz, D. Schiff, Nucl. Phys. B **286**, 553 (1987)
11. R.K. Ellis, J.C. Sexton, Nucl. Phys. B **269**, 445 (1986)
12. C.F.v. Weizsäcker, Z. Phys. **88**, 612 (1934); E.J. Williams, Phys. Rev. **45**, 729 (1934); Kgl. Danske Vidensk. Selskab. Mat.-fys. Medd. **XIII** (1935) N4
13. S. Frixione, M.L. Mangano, P. Nason, G. Ridolfi, Phys. Lett. B **319**, 339 (1993)
14. M. Glück, E. Reya, A. Vogt, Phys. Rev. D **45**, 3986 (1992)
15. H.L. Lai, J. Huston, S. Kuhlmann, F. Olness, J. Owens, D. Soper, W.K. Tung, H. Weerts, Phys. Rev. D **55**, 1280 (1997)
16. S.D. Ellis, D.E. Soper, Phys. Rev. D **48**, 3160 (1993) and references therein
17. L.E. Gordon, J.K. Storrow, Nucl. Phys. B **489**, 405 (1997)
18. J.F. Patrick for the CDF Collaboration, Talk given at the 7th Topical Workshop on Proton Antiproton Collider Physics, Batavia, Illinois (1988) 217
19. B. Combridge, C.J. Maxwell, Nucl. Phys. B **239**, 429 (1984)